Comparison of Three Calibration Techniques for Utilization of GER 63-Channel Aircraft Scanner Data of Makhtesh Ramon, Negev, Israel

E. Ben-Dor, F.A. Kruse, A.B. Lefkoff, and A. Banin

Abstract

Geophysical Environmental Research (GER) 63-channel aircraft scanner data were used to map the mineralogy at Makhtesh Ramon in the Negev area of southern Israel. The data were calibrated to apparent reflectance using three techniques; the flat field (FF) method, the empirical line (EL) method, and the internal average relative reflectance (IARR) method. Results of these calibrations were evaluated by extracting image spectra and comparing them to library spectra for pure minerals and to laboratory spectra of samples collected from the field area. These comparisons show that each calibration method produces apparent reflectance spectra that contain useful mineralogical information. Care must be taken, however, to avoid over interpretation, as all of these calibrations may produce spectral artifacts. For this site, the IARR reflectance technique, which does not require a priori *knowledge, was selected as providing the best results. Mineral maps were produced showing the spatial distribution of several spectral endmembers. Comparison of the mineral maps with laboratory spectral measurements of field samples and published geologic maps indicates that the GER imaging spectrometer data are providing additional geologic detail.*

Introduction

The Geophysical Environmental Research (GER) aircraft scanner system was described in detail by Collins and Chang (1988; 1990). Basically, the instrument provides 63 spectral channels in the visible/near-infrared (VNIR) and shortwave infrared (SWIR) regions with a spectral coverage of 0.433 to 0.971 μm and 1.080 to 2.495 μm, respectively. This spectral coverage is obtained by using three detector arrays for the VNIR (0.433 to 0.971 μm), SWIR1 (1.080 to 1.800 μm), and SWIR2 (1.986 to 2.495 μm) regions with a bandwidth of 12.4 nm, 120 nm, and 16.2 nm, respectively. This instrument is, in effect, an imaging spectrometer in that it provides high-resolution, near-laboratory-quality reflectance spectra for each pixel of the image.

GER aircraft scanner data have been used successfully for a number of mineralogical applications since 1985 when the first results of a narrow-band scanner were reported by Collins and Chang (1985). In Australia, Mackin and Munday (1988) concluded that the instrument is capable of distinguishing between Al-OH, Mg-OH, and carbonate minerals and can be used effectively for remote mineral identification. Using GER data, Podwysocki and Jones (1988) mapped out distributions of kaolinite, alunite, and buddingtonite at Cuprite, Nevada. Kruse *et al.* (1988; 1990), working in the same area, concluded that using imaging spectrometers such as GER allowed production of detailed maps for mineral exploration. They pointed out that, in addition to the minerals mapped by Podwysocki and Jones (1988), hematite, goethite, and jarosite could be mapped at Cuprite without prior knowledge of their locations. Werner and Lehmann (1991) concluded that soil surfaces with even small mineralogical variation could be differentiated using the shortwave infrared (SWIR) GER data. All of these applications emphasized the requirement for adequate calibration to reflectance of the raw GER data. This step is perceived as critical for deriving maximum information from such data (Vane *et al.*, 1987).

The GER instrument was flown over Makhtesh Ramon, Negev Israel during July 1989. Unfortunately, the flight was not followed by field reflectance measurements nor any ground sampling. Except for one recent study (Kaufmann *et al.*, 1991), the data have not been analyzed, mostly because of calibration difficulties. Kaufmann *et al.* (1991) have applied the flat field (FF) and/or log residual (LR) calibration methods to part of the second flight line (from four taken) for the SWIR region only. Different GER spectra obtained for different lithological units were presented; however, no sup-

E. Ben-Dor is with the Center for the Study of Earth from Space (CSES), Cooperative Institute for Research in Environmental Science (CIRES), University of Colorado, Boulder, CO 80309-0449; and the Faculty of Agriculture, Hebrew University of Jerusalem, Rehovot, Israel.

F. A. Kruse is with the Center for the Study of Earth from Space (CSES), Cooperative Institute for Research in Environmental Science (CIRES); and Department of Geological Sciences, University of Colorado, Boulder, CO 80309-0449.

A.B. Lefkoff is with the Center for the Study of Earth from Space (CSES), Cooperative Institute for Research in Environmental Science (CIRES), University of Colorado, Boulder, Co 80309-0449.

A. Banin is with the Faculty of Agriculture, Hebrew University of Jerusalem, Rehovot, Israel.

Photogrammetric Engineering & Remote Sensing, Vol. 60, No. 11, November 1994, pp. 1339–1354.

0099-1112/94/6011-1339$3.00/0

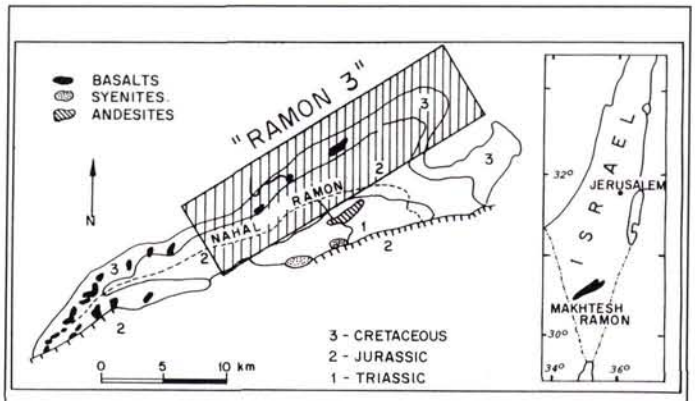

Figure 1. Makhtesh Ramon: location and geology (after Zak (1987)) and coverage of the Ramon-3 flightline.

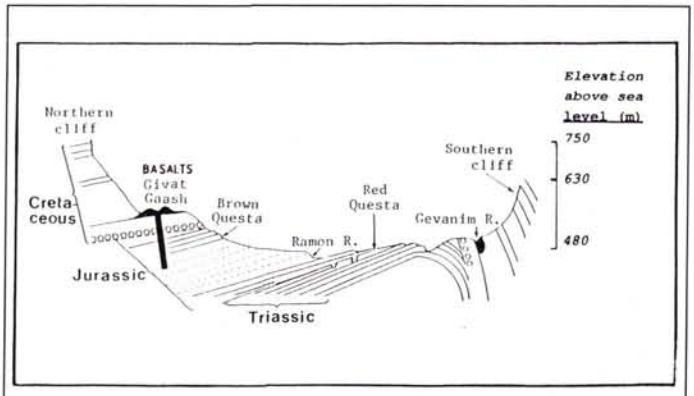

Figure 2. Schematic cross section of central Makhtesh Ramon (after Mazor and Shoval (1987)).

porting spectral measurements were presented and detailed information about the calibration methods was not discussed.

This study compares three commonly used calibration methods (the flat field (FF) method, the empirical line (EL) method, and the internal average relative reflectance (IARR) method) for the GER data of Makhtesh Ramon. The study covers the full VNIR-SWIR (0.4- to 2.5-μm) region and uses ground sampling for verification checks. The purpose of this study was to provide a baseline to help future workers achieve the most from this particular GER flight and to provide general information regarding the applicability of specific calibration methods to the GER data.

Geology and Alteration

Makhtesh (mortar in Hebrew) Ramon is located in southern Israel in the Negev area (Figure 1). Structurally, the area is an anticline with an eroded central valley, mostly drained by a single river (Nahal Ramon). The valley is bounded by steep walls with friable sandstones at the bottom and more resistant limestones and dolomites at the top (Ben-David and Mazor, 1988) (Figure 2). Makhtesh Ramon shows a continually exposed section from the Middle Triassic to the Middle Eocene. A good geologic summary (paraphrased below) is given by Kaufmann *et al.* (1991).

The Triassic formations at Makhtesh Ramon consist primarily of sandstones and marine-littoral shales overlain by alternating limestones, dolomites, and argillaceous carbonates ("marl"). The Upper Triassic sediments are interpreted as lagoonal and are characterized by intercalated gypsum, dolomite, and clay capped by limestones. Jurassic sediments unconformably overlay the Triassic with development of fossil laterites consisting mainly of kaolinite and bauxite minerals prior to deposition of the Jurassic units. The Lower Jurassic Ardon formation was deposited in a shallow-water marine environment. The Early to Middle Jurassic Inmar formation consists primarily of sandstones and lacustrine clays and is overlain by sandstones, dolomite, and shales. A major unconformity separates the marine sediments of the Middle Jurassic from the continental Nubian sandstones of the Early Cretaceous Hatira Formation. Upper Cretaceous limestones and dolomites contain glauconite and bentonite beds. Alkaline to hyper-alkaline laccoliths, sills, and dikes have been intruded into all units up to the Early Cretaceous. Hydrothermal alteration is often associated with these intrusions. Large sheet extrusions of alkaline basalts took place during the Early Cretaceous. There are limited exposures of Eocene limestones on the southern side of the makhtesh.

Evolution of the present exposure of Makhtesh Ramon is the result of post-Eocene erosion and structural modification. Ben-David and Mazor (1988) present evidence for the formation of a pre-makhtesh peneplane during the Miocene caused by rivers flowing from south to north. They attribute excavation of the makhtesh by an eastward-flowing fluvial system to subsidence of the Arava Rift Valley accompanied by eastward tilting of the Negev heights including the Ramon monocline, the pre-makhtesh peneplane, and Hatira Formation sandstone exposures. Subsequent deepening of the Makhtesh resulted from gradual erosive incision, forming step-like alluvial terraces. Neotectonic movements along predominantly east-west dextral strike-slip structures are recorded in shifts of the course of Nahal Ramon. Wind-borne sediment from the loess province of the northwest Negev has been trapped at the makhtesh walls (especially the northwest walls) and stabilized by debris (Ben-David and Mazor, 1988).

The area of Makhtesh Ramon is known as one of the most important mineralogical sites in Israel and is termed as a "laboratory in nature" (Ben-David and Mazor, 1988). The area has been declared a "Reserve National Geology Park" and consists of interesting mineralogical variation exposed in a small area. Because of the arid weather, only minor vegetation occurs within the Makhtesh. As a result, the area was selected to be covered by the GER aircraft scanner in order to yield new, useful information regarding the lithology and mineralogy of the Makhtesh Ramon.

The Calibration Methods

Because the GER system responds to solar irradiation and atmospheric attenuation and scattering as well as Earth's surface reflectance, it is critical to remove unwanted components of the signals prior to analysis. The atmospheric/irradiation removal procedure (so called calibration) is an important step that must be taken prior to any spectral image analysis. This step requires great attention and care, and requires careful study for each image data set. This stage is doubly important for the GER scanner data because no onboard calibration is available. Several methods to calibrate high resolution image data are in common use. Methods selected for this study and useful for unvegetated areas are discussed below:

(1) The **Flat Field** (FF) method has been widely applied in studies involving imaging spectrometer data (Goetz and Srivastava, 1985; Conel, 1985; Crowley *et al.*, 1988; Rast *et al.*, 1991). This method requires a small area in the scene characterized by non-absorbing materials. The average spectrum of the small area is then divided into the spectrum for every pixel in the scene to achieve a normalized image. This method suffers difficulties related to defining a homogeneous area (spectrally featureless area) within the scene being studied.

(2) The **Empirical Line Method** (EL) method is a useful technique for removing the atmospheric and solar effects as well as instrument noise. This technique is described in detail by Roberts *et al.* (1985) and has been successfully applied by several other workers (Conel *et al.*, 1988; Elvidge, 1988; Green *et al.*, 1988; Kruse *et al.*, 1990; Zamudio and Atkinson, 1990). Basically, the method requires field or laboratory spectra for two targets of contrasting albedo and several imaging spectrometer radiance spectra for each of the two ground targets. A linear regression is used to force the response of each image spectral channel to match the field spectra of the two targets, and the atmospheric-solar-instrument factors are determined as gains and offsets to be applied to the data. These factors are used to transform instrument DN into reflectance for the entire imaging spectrometer data set.

(3) The **Internal Average Relative Reflectance** (IARR) method is described in detail by Kruse *et al.* (1985) and Kruse (1988). This method uses a reference spectrum curve calculated as the spectrum average of the whole imaging spectrometer scene. This curve is then divided into each image radiance spectrum to produce a residual relative reflectance curve for each pixel. Although the IARR method does not require previous knowledge of the study area, great attention must be taken when interpreting the spectra (Kruse, 1988). As in the case of the Flat Field method, artifacts may be interpreted as real spectral features and individual absorption features may be suppressed or removed, depending upon the spectral response of the dominant cover types (Kruse, 1988; Mackin and Munday, 1988; Zamudio and Atkinson, 1990).

While ground sampling and field-laboratory spectral measurements (which ideally should be taken very close to the flight time) are a basic condition to use for calibration of method 2, no field-laboratory measurements are required for methods 1 and 3. Calibration method 1 can technically be run without field-laboratory measurements and even produce reasonable results if techniques such as "relative band depth" (RBD) are applied (Crowley, 1990). In practical use, however, this method requires *a priori* spectral knowledge of the study area for accurate selection of featureless targets.

There are other equally viable calibration methods besides the three calibration methods discussed here. These methods include techniques with similarities to the above methods and other model-based techniques. Several having similarities are the Single Spectrum (SS) method (Crowley *et al.*, 1988), which requires field measurements, and the Log Residuals (LR) method and Least Upper Bound (LUB) methods (Green and Craig 1985). Other techniques based upon atmospheric models, such as the LOWTRAN-7 model (Kneizys *et al.*, 1988; Rast *et al.*, 1991), require atmospheric measurements taken during the flight. Other techniques that use atmospheric models and information from the imaging spectrometer data themselves are also providing excellent calibration results (Gao and Goetz, 1990). For all calibration methods, verification is a very important stage that has to be accomplished routinely in order to prevent errors in the image interpretation.

Data Processing and Analyses

Data Characteristics

The GER aircraft was flown over Makhtesh Ramon on 9 July 1989. Four flight lines were flown to cover most of the Makhtesh Ramon area. One flightline was flown at an altitude of approximately 1500 metres (5000 ft) above sea level and was named Ramon 1. The data from this flightline are severly distorted because of synchronization problems which occurred between the aircraft and the scanner motions. The other three flightlines were flown at an altitude of approximately 4500 metres (15,000 ft) and named Ramon 2, 3, and 4. For this study, only flight line Ramon 3 was selected (Figure 1). This flight was characterized by the following data: flight direction, 050°; starting local time, 1050; flight time, 5 minutes; starting geographic points (in terms of the local Israeli geographic system), 1225,9976; and flight altitude, 4500 metres. Data were recorded in 16-bit mode and each cross-track consisted of 512 pixels. The ground resolution obtained was about 13.44 m by 13.44 m at nadir. System parameters for the whole spectral region (including number of bands, band-width, and band centering) are given in Tables 1 and 2 (Kaufmann *et al.*, 1991). Two bands were omitted from the analysis (band 28, 0.81 μm, and band 32, 1.440 μm) because of poor (noisy) spectral response. Band centering was examined on the basis of known absorption features of the atmospheric carbon dioxide (CO_2) located at 2.005 and 2.055 μm. The corresponding CO_2 bands were observed in the GER radiance data at 2.002 μm and 2.054 μm, thus confirming the nominal values provided by GER. As other strong absorption bands (such as CO_2) are absent in the VNIR region with respect to the GER raw data, we assume that band centering is accurate throughout all the GER spectral regions.

Interactive Data Viewing and Analysis

An updated version of the Spectral Image Processing System (SIPS v 1.1) developed at the Center for Study of Earth from Space (CSES) was used to read and process the GER data (CSES, 1992; Kruse *et al.*, 1993). This sophisticated and user-friendly package provides many interactive analysis tools such as data calibration, image display and enhancement, color compositing, selection and display of image spectra, region of interest analysis, spectrum matching, and more (Kruse *et al.*, 1993). The package includes two spectral libraries: the IGCP-264 library (Kruse and Hauff, 1993) and the JPL Spectral Database (Grove *et al.*, 1992) which together contain more than 180 laboratory spectra, primarily of pure minerals. Additionally, the software allows users to create their own spectral libraries and permits interactive comparison between the image spectra and the library spectra. For the current study, all 197 laboratory spectra (26 IGCP-264, 160 JPL, and the 11 spectra measured in the laboratory for the Ramon site) were resampled into the 63 GER channels to allow improved comparison between the GER and the library spectra. The spectra related to the IGCP-264 or to the JPL Database were named "LIB" and those related to the Ramon spectral library were named "LAB."

In order to preview the data (prior to the calibration process), each of the 63 GER channels of the "Raw" (uncalibrated) data were examined. Channel #45 is shown in Figure 3 as an example of a typical image. Comparison of this image to Figures 1 and 2 allows location of many of the mapped geologic features and stratigraphic units. Note that there are several clouds on the west part of the image. The

TABLE 1. WAVELENGTHS AND CALIBRATION FILE FOR THE MAKHTESH RAMON FLIGHT, JULY, 1989 (SOURCE, LEHMANN ET AL. (1990 TAKEN FROM KAUFMANN 1991)).

	VNIR				SWIR		
channel	center wavelength [nm]	center wavenumber [cm^{-1}]	calibration file [$mWcm^{-2}\ sr^{-1}\ \mu m^{-1}$]	channel	center wavelength [nm]	center wavenumber [cm^{-1}]	calibration file [$mWcm^{-2}\ sr^{-1}\ \mu m^{-1}$]
1	477	20964	0.0539	32	1400	—	—
2	489	20450	0.0584	33	1560	6410	8.54 E-4
3	502	19920	0.0562	34	1680	5952	1.08 E-3
4	514	19455	0.0474	35	1800	5555	2.10 E-4
5	526	19011	0.0429	36	2005	8	3.27 E-4
6	539	18553	0.0417	37	2022	4946	6.27 E-4
7	551	18149	0.0342	38	2038	4907	6.51 E-4
8	564	17730	0.0426	39	2054	4869	4.86 E-4
9	576	17361	0.0395	40	2070	4831	4.84 E-4
10	588	17007	0.0386	41	2087	4792	6.12 E-4
11	601	16639	0.0359	42	2103	4755	5.77 E-4
12	613	16313	0.0378	43	2119	4719	5.63 E-r
13	625	16000	0.0343	44	2135	4684	6.01 E-4
14	638	15674	0.0318	45	2151	4649	5.48 E-4
15	650	15385	0.0305	46	2168	4613	5.83 E-4
16	662	15106	0.0291	47	2184	4579	5.61 E-4
17	675	14815	0.0301	48	2200	4545	5.48 E-4
18	687	14556	0.0226	49	2216	4513	6.30 E-4
19	699	14306	0.0274	50	2232	4480	6.55 E-4
20	712	14045	0.0252	51	2249	4446	6.14 E-4
21	724	13812	0.0236	52	2265	4415	6.30 E-4
22	736	13587	0.0240	53	2281	4384	6.22 E-4
23	749	13351	0.0257	54	2297	4354	5.70 E-4
24	761	13141	0.0250	55	2314	4322	5.36 E-4
25	774	12920	0.0234	56	2330	4292	5.14 E-4
26	786	12723	0.0227	57	2346	4263	5.96 E-4
27	798	12531	0.0143	58	2362	4234	7.21 E-4
28	811	—	—	59	2378	4205	6.47 E-4
29	823	12151	0.0124	60	2395	4175	6.70 E-4
30	835	11976	0.0184	61	2411	4148	6.88 E-4
31	848	11792	0.0165	62	2427	4120	8.02 E-4
				63	2443	4093	7.46 E-4

associated cloud shadows (black) could easily be mistaken for basalt. All ground locations and targets discussed throughout this report (for calibration, and verification as well) are also shown on this image.

Ground Sampling and Calibration Sites

Selected ground sites (see Figure 3) along the flightline were sampled during June 1992. Rock and soil samples were collected, and measured in the laboratory using a GER Single beam Infrared Intelligent Spectrometer (SIRIS) (GER, 1988). The SIRIS is a grating spectrometer that measures reflectance from 0.4 to 2.5 μm at approximately 4-nm band centers (this is the sampling interval, not the true resolution). Spectra were measured using quartz-halogen illumination and HALON as a reflectance standard. HALON is a highly reflective material with no absorption features in the 0.4 to 2.5 μm range (Weidner and Hsia, 1981). Mineral verification for each sample was accomplished using X-Ray diffraction (XRD) analysis. The instrumentation (Scintag Inc. machine, CuKa radiation) and the method used (automatic powder measurements) are described by Mckie and Mckie (1986). For the current study we used a scanning rate of 2°/min. from 2 to 55° and unoriented ground ("flour like") powders (except for 3G where the rock surface was also scanned). All ground locations for both calibration and verification are described below:

- *Flat Field calibration sites*
  (I) DARK - A dark target selected on "Givat Gaash." This location consists of basalt and was used for the flat field calibration as a dark target. Also, this location was used for the signal-to-noise examination in all calibrations.

TABLE 2. SYSTEM PARAMETERS OF THE GER SCANNER AND OTHER PARAMETERS FOR THE RAMON-3 FLIGHTLINE.

• Wave-bands:	63 with selectable wavelength
• Dynamic range:	16 bits radiometrically calibrated
• Signal-to-noise:	VNIR - range to 5000 SWIR - range to 500
• IFOV:	selectable 2.5 to 4.6 mRad 3.3
• Pixels per scan:	selectable 512 to 1024
• Scan speed:	selectable 1 to 50 scans per sec.
• Current design:	Makhtesh Ramon/ISRAEL
VNIR - Module:	477 - 848nm: 31 bands sampling interval: 12.37nm
SWIR 1 - Module:	1440 - 1800nm: 4 bands sampling interval: 120nm
SWIR 2 - Module:	2005 - 2443nm; 28 bands sampling interval: 16.22nm
Date/ Local-Time	09 July 1989/1050 hr
Flight Altitude (a.s.l.):	15,000 feet
GIFOV at 3.3 mRad:	13.44m at Nadir
Flight Direction:	050 ° az.
Mean Sun Elevation	78.3°

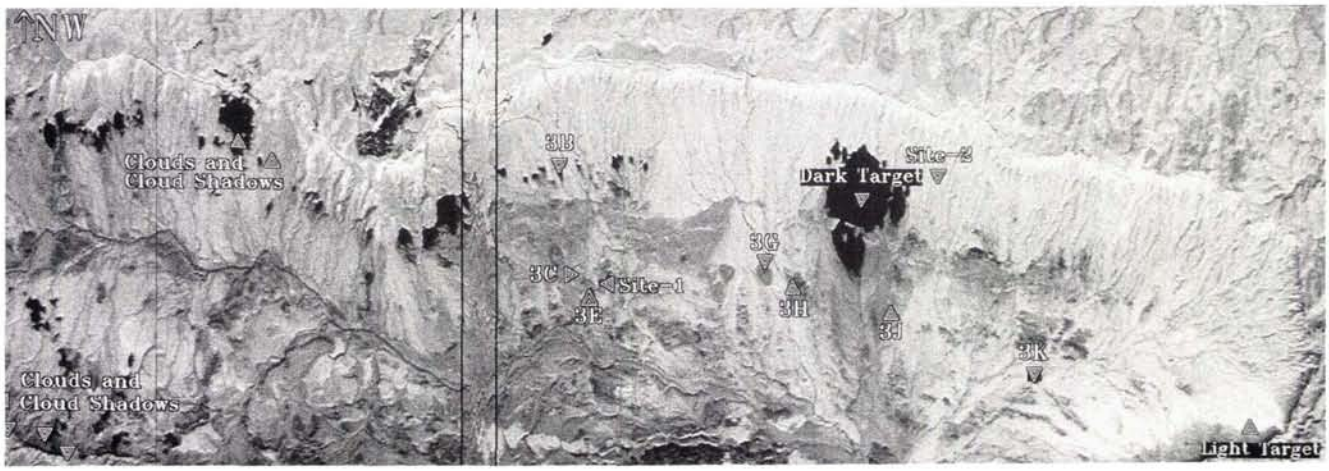

Figure 3. Gray-scale image of Ramon-3 flightline, channel 45. Also shown are ground locations for calibration, verification, and mapping. The area between the two black lines contains damaged pixels due to aircraft role distortion (Lillesand and Kiefer, 1979).

(II) LIGHT - A light target selected on "Biqa'at Mahmal." This location consists of quartzitic sandstone and was used for the flat field calibration as a light target. Also, this location was used for the signal-to-noise examination in all calibrations.

- *Verification sites*
  (I) Ground locations marked as 3B, 3C, 3E, 3G, 3H, 3J, and 3K were located along the flightline direction as mentioned previously and shown in Figure 3. Samples were measured in the laboratory using the SIRIS, and their spectra were used to verify the GER spectra obtained from each calibration.
  (II) Ground targets "Site-1" and "Site-2" are located on two different geologic formations. Site-1 is on a kaolinite quarry (also known as a "flint clay" quarry) from the Jurassic Inmar formation. Site-2 is located east of Givaat Gaash on the northwest side of the Makhtesh Ramon wall in the Cretaceous, Hatira formation.

Calibration Procedures

The flat field (FF) calibration was done using both a light target and a dark target for comparison. The Light Target (Figure 3) contained 10 by 10 homogeneous pixels which were averaged to yield a "high albedo" reference curve. This reference curve was then used as the denominator to divide into each image spectrum (pixel) to produce the Flat Field corrected "LIGHT" calibrated data (FF1). The Dark Target (Figure 3) was also selected with 10 by 10 homogeneous pixels to yield a "low albedo" reference curve. Again, this reference curve was divided into each pixel's spectrum to produce the Flat Field corrected "DARK" calibration data (FF2).

The empirical line (EL) calibration was performed according to Kruse *et al.* (1990) using the SIPS utilities *"make gainoff"* and *"dn2ref"* (CSES, 1992). In this calibration we interactively selected two geographically close targets with contrasting albedos (3B and 3C) situated at about the average elevation of the scene. The laboratory spectra of the two EL ground sites (resampled into the 63 GER channels) are presented in Figure 4. In general, the two spectra accurately represent the known mineralogy of the high (3C) and low (3B) albedo targets. Sample 3B is a dark basalt and sample 3C is a light quartzitic sandstone. The general mineralogy of both sites was verifyed in the field. However, from Figure 4 it can be seen that, in the laboratory, the reflectance spectrum of sample 3C shows some kaolinite impurities (as demonstrated by the absorption features at around 2.2 μm).

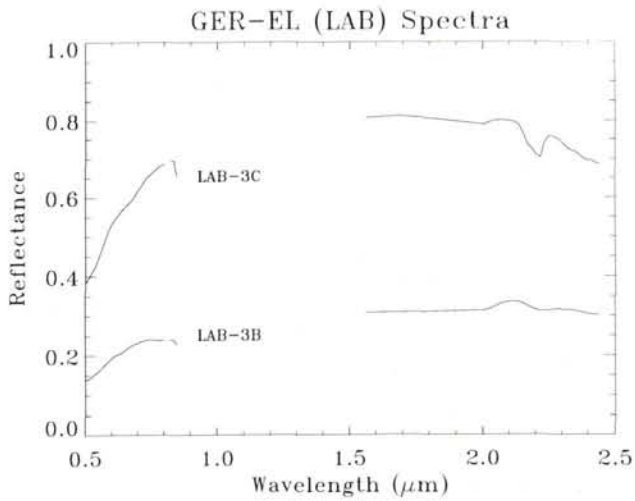

Figure 4. Laboratory spectra of the two EL targets (3B and 3C) resampled into the GER 63 channels.

For the EL calibration, several pixels (spectra) were extracted from the GER data for each target. A linear regression revealing the relation between the DN for the dark and light targets and reflectance was performed using the multiple image spectra and the single laboratory spectrum for each target. The calculated slope and intersect correspond to gains and offsets required for each spectral band to force the image spectra to look like the laboratory spectra. The correction of the instrument digital numbers (DN) into reflectance values

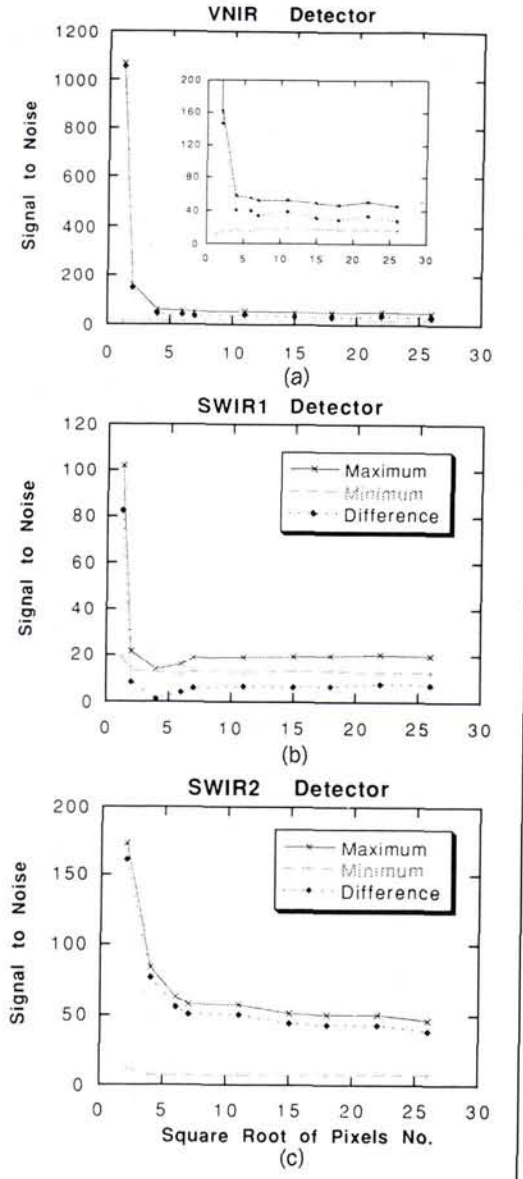

Figure 5. Signal-to-noise values of the maximum, minimum, and their differences (DIF) of the VNIR (a), SWIR1 (b), and SWIR2 (c) detectors versus the square root of the pixel number selected for this analysis. The pixels were selected from the LIGHT target presented in Figure 3.

was done by applying the proper gain and corresponding offset values to the instrument DN values to yield the EL calibrated data.

The internal average relative reflectance (IARR) calibration was performed according to Kruse *et al.* (1985) and Kruse (1988) with the exception that an equal energy normalization was not applied to the data. In this calibration, a global average spectrum for the scene was calculated by taking the simple average of all of the image spectra (all pixels). This single reference curve was then used as the denominator and divided into each raw spectrum to produce a new relative spectrum for each of the pixels. The result of this procedure is the IARR calibrated GER data set.

Signal-to-Noise Analyses

The signal-to-noise ratio (SNR) was estimated by calculating the average (X) and the standard deviation (σ) of several (n) pixels' spectra according to the following equation:

$$SNR = \frac{\overline{X}_n}{\sigma_n} \quad (1)$$

The raw image data were first used to study the relationship between the SNR and the number of pixels in the analysis (n) for both the FF1 and FF2 targets. In order to obtain an accurate representation of the SNR with respect to wavelength, we divided the GER spectrum into three major parts corresponding to the three detectors onboard (VNIR, SWIR1, SWIR2). For this SNR calculation, we selected the "LIGHT" target for the study area. Figures 5a, 5b, and 5c present values of the maximum, minimum, and their differences (DIF) SNR values within each detector wavelength range versus the square root of the pixel number (for emphasizing the changes). Similar trends are observed for the three detectors; a sharp decrease of the maximum SNR values, going from 2 (1.41^2) to 36 (6^2) pixels and a stabilization of the SNR at >36 (6^2) pixels. For the minimum SNR values, a stable trend across all pixel numbers is obtained. The difference between the maximum and the minimum SNR values (DIF) is large for the VNIR and SWIR2 detectors and somewhat smaller for the SWIR1 detector. The DIF SNR values, which represent the noise amplitude, actually indicate the quality of the data. Where this value is low (accompanied by relatively high SNR value), the data quality is high. According to the above, the VNIR detector provides reasonable performance using >16 (4^2) pixels, the SWIR1 detector provides reasonable performance using >4 (22) pixels, and the SWIR2 provides reasonable performance using >64 (8^2) pixels. The high SNR values obtained by using only 2 (1.41^2) pixels for SNR calculation (SNRs of 1068 for VNIR, 101 for the SWIR1, and 173 for the SWIR2) do not represent high spectral accuracy. To the contrary, the corresponding high DIF values (1057, 83, and 162, respectively) suggest low data quality. These high SNR values are only high because of the typical close correlation of two adjacent pixels and the nature of the SNR calculation. An average of two close pixels usually has a low standard deviation and therefore the SNR is high. Although Collins and Chang (1990) reported an SNR of 500:1 for the GER data, we believe that their high SNR values cannot be practically used without reporting the DIF SNR values. For the same GER flight (but for a different flight line (Ramon 2)), Kaufmann *et al.* (1991) reported that the SWIR detector yielded maximum SNR values of about 50:1. Although we used uncalibrated data, a different flight line (Ramon 3), and different targets, Kaufmann's maximum SNR value is in good agreement with our maximum SNR values for targets of similar spatial dimensions.

According to the previous discussion and by assuming that it is impossible to find natural surfaces showing real homogeneity within a large area, we selected the configuration of 64 pixels for further SNR study. We compared the SNR values of the raw data and four calibrated data sets (IARR, EL, FF1, and FF2). Figure 6 presents the SNR values versus the wavelength for these images using the DARK and LIGHT targets. Similar results were obtained for the Raw, IARR, FF1,

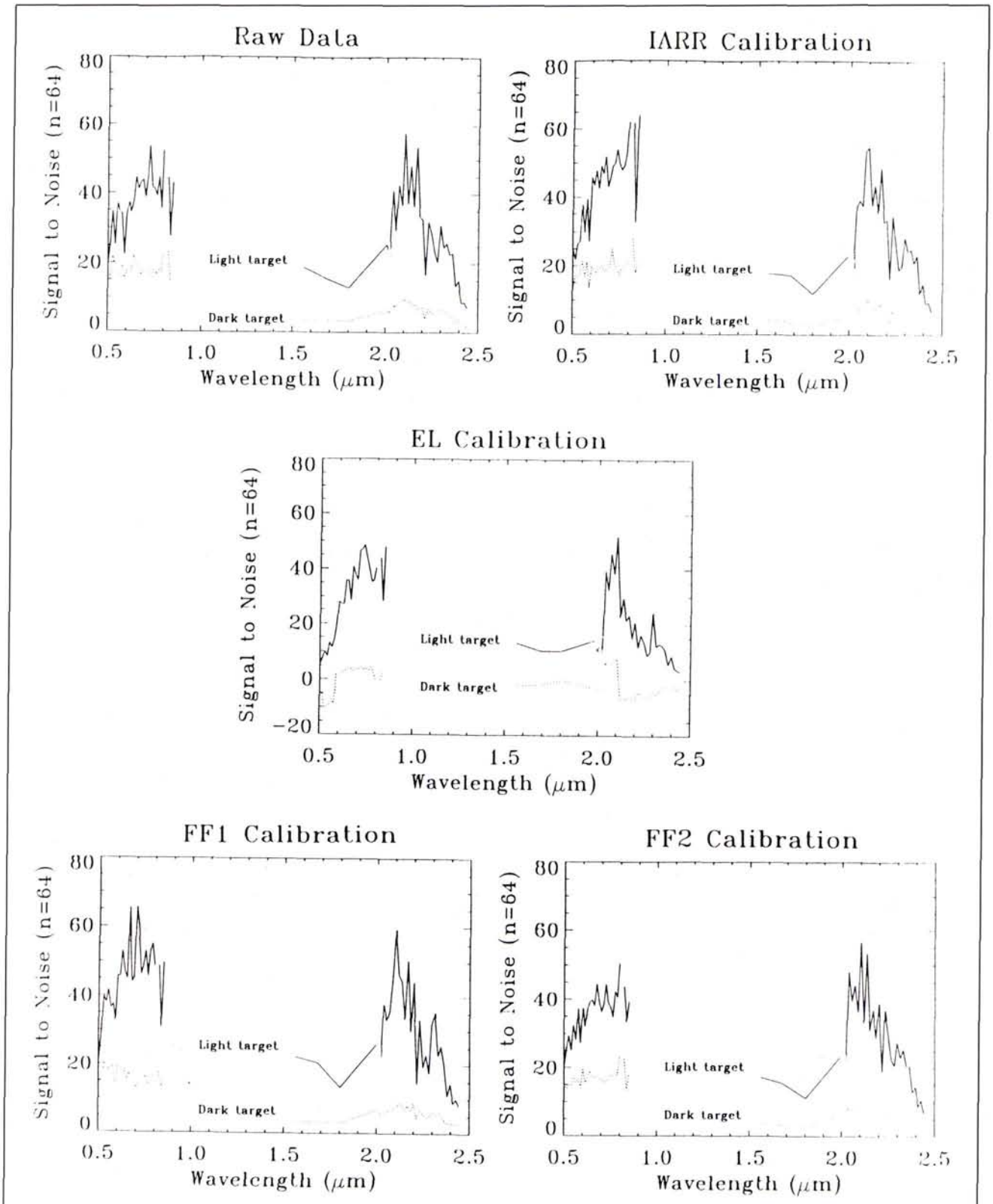

Figure 6. Signal-to-noise values derived from 64 pixels for the DARK and the LIGHT targets (presented in Figure 3 as Dark and Light Target, respectively) and for the uncalibrated (Raw) and calibrated (IARR, EL, FF1, and FF1) data.

TABLE 3. MAJOR MINERALS IN THE SAMPLES AS DETERMINED BY USING XRD.

Sample	Minerals
3C	Quartz (++++), Kaolinite (++), Goethite (+)
3E	Kaolinite (++++), Quartz (++), Goethite (+)
3G	Quartz (++++), Kaolinite (minor - detected on the rock surface only)
3H	Kaolinite (++++), Muscovite (++), Calcite (+)
3J	Calcite (+++), Dolomite (+++), Hematite (+)
3K	Kaolinite (+++), Quartz (++), Calcite (+), Hematite (+), Goethite (+)

and FF2 calibrations. The EL calibration shows a lower SNR throughout the whole spectral region and particularly for the DARK target. This examination suggests that precautions must be taken when applying the EL calibration. This calibration appears to perform poorly in the 0.5- to 0.6-μm and 2.1- to 2.5-μm regions for dark (low albedo) materials.

Verification of the Calibrations

Comparison to Laboratory Spectra

Six ground locations were used to verify the calibrations (3C, 3E, 3G, 3H, 3J, and 3K). Samples were taken from the upper centimetre of the surface within an area of about 2 m^2. Samples were selected to best represent the lithological units exposed in the field. For verification purposes, first, the mineralogy of each sample was determined using XRD. Then the laboratory reflectance spectrum of each sample was compared to spectra of the minerals identified using the XRD taken from the SIPS spectral libraries. Table 3 shows the major mineral compositions determined by XRD analysis. Figure 7 compare the SIRIS laboratory reflectance spectra (LAB) of each sample to spectra of end-members taken from the SIPS libraries (LIB) for each of the XRD-identified components. In general, good matches are obtained between the LAB and the LIB spectra (spectral features present in the LIB spectra can be seen in the LAB spectra). The SWIR region is very sensitive to small amounts of kaolinite and carbonate (both calcite and dolomite). The VNIR region in most of the samples allows identification of the iron oxides (hematite and goethite). Because quartz is almost transparent to the VNIR-SWIR radiation, small amounts of kaolinite in sample 3G (that were detected by XRD on the rock surface but not in the ground powder; see Table 3) can be detected using the reflectance spectroscopy. Comparison of the LAB and LIB spectra for samples 3H and 3K, however, indicates that, in mixtures where the main absorption bands appear in the SWIR, some of the XRD-identified components can not be identified based upon absorption features using the spectroscopy.

Figures 8 through 13 compare the GER (IARR, EL, FF1, and FF2 calibrated) spectra of the six ground sites to the best SIRIS laboratory spectra of the corresponding samples. Significant absorption features appearing in all samples in the SWIR2 region are caused by kaolinite or carbonate at the ground locations. The absorption bands around 2.2 μm can be assigned as a combination of the fundamental Al-OH vibration in kaolinite ($\nu_{OH\text{-}Al}+\delta_{OH\text{-}Al}$; Hunt and Salisbury, 1970). Accordingly, the absorption band around 2.3 μm can be assigned as an overtone and combination of fundamental vibration of CO_3 in carbonates ($3\nu_3$; Gaffey, 1986). In most of the targets (except for 3H), the IARR calibration for the SWIR2 region gives the best match to the laboratory spectra. Ground location, 3H, shows a noisy spectrum throughout the entire spectrum in all calibrations. This is caused by the limited size of this target which limited the number of pixels selected for this particular analysis to 28 which is less than the recommended limit ($n = 64$).

Although the IARR calibrated spectra somewhat match the VNIR and SWIR1 regions, the EL calibration appears to provide better matches to the laboratory spectra in these particular regions (omitting 0.5 to 0.6 μm and 2.3 to 2.5 μm because of high noise). The FF2 calibration also provides good spectral matches in the VNIR region. In all samples it is clearly seen that the VNIR region holds significant spectral information and hence represents a region of a great interest. The presence of significant VNIR absorption bands in the GER data suggests that at Makhtesh Ramon, Fe-bearing minerals are playing as important a role as the CO_3 and OH-bearing minerals.

Comparison to Library Spectra

As mentioned previously, two targets were selected to verify the best calibration: Site-1 and Site-2. Verification was accomplished by comparing the calibrated GER spectra to IGCP-264 library spectra. Figure 14 shows the GER radiance spectra of these two sites as derived from 125 pixels *before* calibration was applied. Although clearly there is some evidence of an absorption feature near 2.2 μm in the Site-1 spectrum, no mineral identification is possible. The strong absorption in both spectra at around 2.0 μm relates to atmospheric H_2O and CO_2 and dramatically demonstrates the requirement for calibration for mineralogical applications. Without atmospheric corrections, the atmospheric absorption features are of greater magnitude than those caused by molecular processes in minerals. Figures 15 and 16 show the GER spectra of the same 125 pixels, after IARR, EL, FF1, and FF2 calibrations were applied. All calibrations for Site-1 produced spectra that more-or-less match the IGCP library spectrum of kaolinite (KL500). While the spectral resolution of the GER instrument is not adequate to resolve the fine detail of the kaolinite spectrum, the position and asymmetry of the feature are adequate to identify kaolinite even at this resolution (Kruse *et al.*, 1988; Hauff and Kruse, 1990). All calibrations for Site-2 produced spectra that match the IGCP-264 library spectrum of calcite (CO2004). The spectrum of dolomite (COD2005) is also shown to demonstrate the small absorption feature offset between calcite and dolomite.

Again, the spectra obtained by applying the IARR calibration appear to provide the best match to the IGCP-264 library spectra in the SWIR2 region. The degree of match is seen clearly in Figures 15 and 16 and emphasized in Figure 17 where the IARR and LIB spectra of the two targets are directly compared. As previously observed when comparing the GER and the LAB spectra, the EL calibrated spectra provide the best match in the VNIR and SWIR1 regions. Despite this, because the EL method provides poor SNR performance in the critical 2.0- to 2.4-μm region, the IARR calibrated data is recommended as the preferred technique for calibration of the GER data in arid to semi-arid terrains.

One additional factor, the effect of spectral averaging, should be considered as pointed out by the SNR analyses. Accordingly, spectra for Site-1 from the IARR calibration were averaged for selected groups of from 2 to 484 pixels and compared to the kaolinite library spectrum. Figure 18 shows that the general shape of the absorption feature remains constant with suppression of noise as expected. No dramatic improvement in the spectrum is observed at averages of >64 pixels.

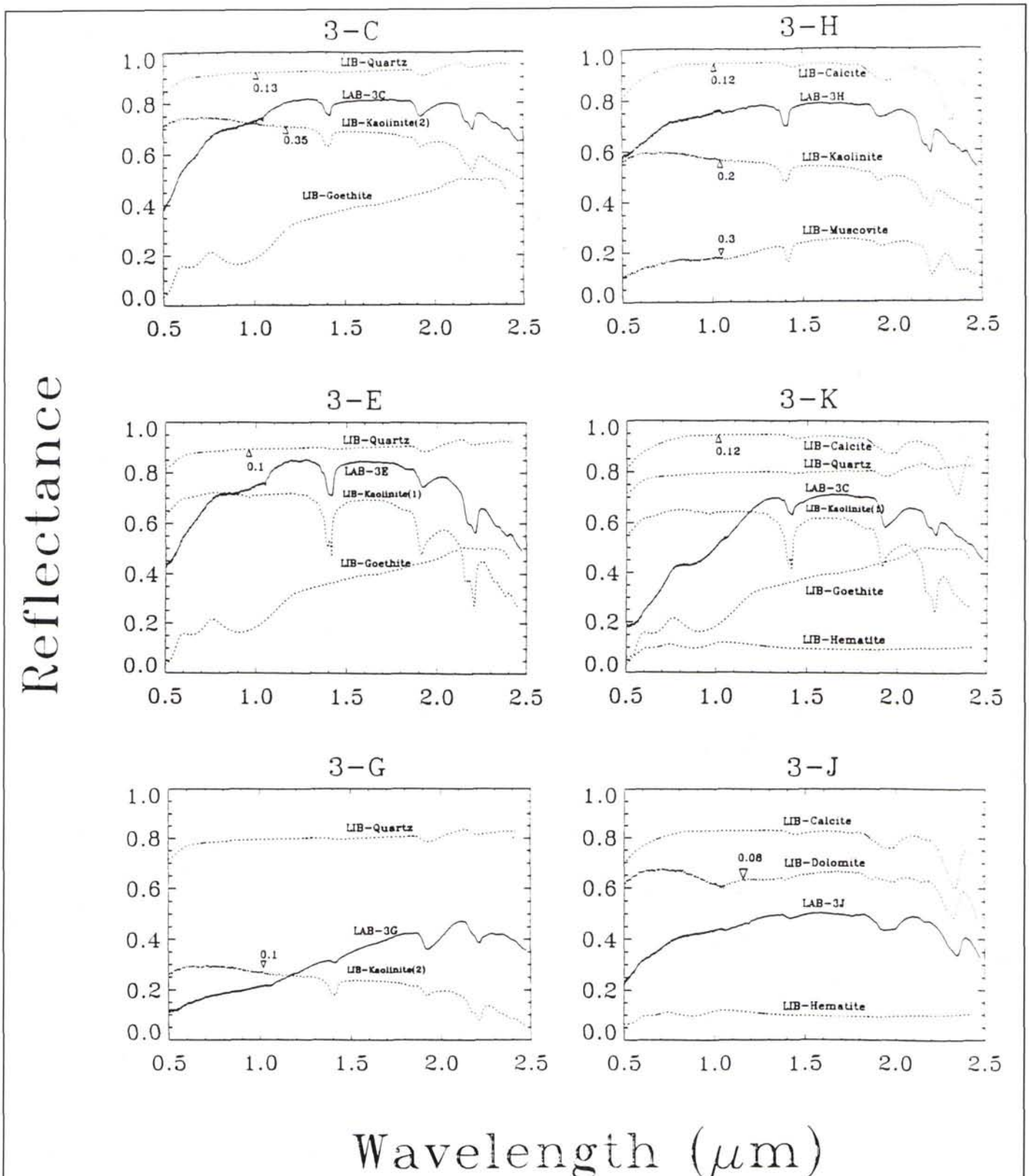

Figure 7. SIRIS library spectra (LIB) of endmembers found in samples 3C, 3E, 3G, 3H, 3K, and 3J (according to Table 3) and the laboratory spectra (LAB) of these samples. Note that some LIB spectra were offset up (Δ) or down (∇) for clarity using the indicated reflectance values.

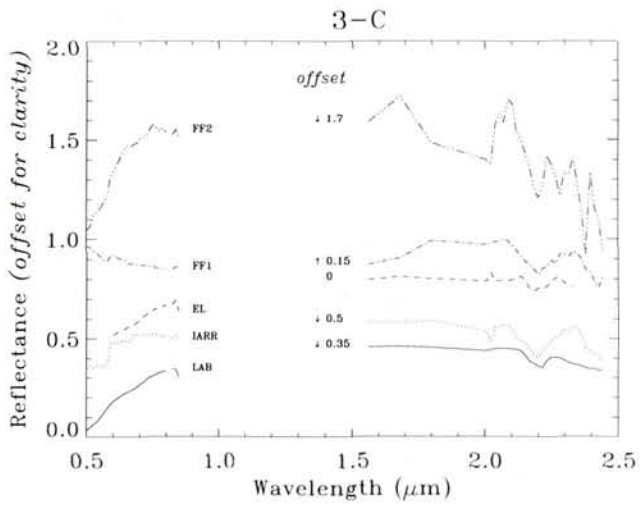

Figure 8. GER spectra for ground location 3C obtained by applying the four calibration methods (IARR, EL, FF1, and FF2). Each of the spectra was derived from exactly 75 pixels. Also shown is a laboratory spectrum of this location (LAB) resampled into the 63 GER channels. Spectral offsets have been applied to the original spectra position (0) for clarity using different reflectance values and magnitude (**E**) as noted in the figure between 1.4 and 1.5 μm.

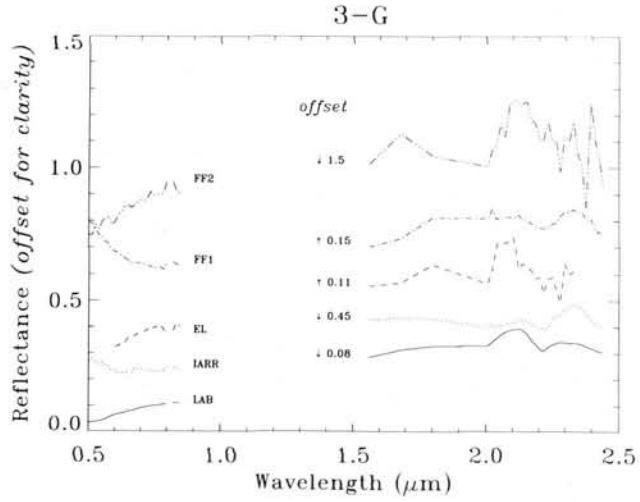

Figure 10. GER spectra for ground location 3G obtained by applying the four calibration methods (IARR, EL, FF1, and FF2). Each of the spectra was derived from exactly 70 pixels. Also shown is a laboratory spectrum of this location (LAB) resampled into the 63 GER channels. Spectral offsets have been applied to the original spectra position (0) for clarity using different reflectance values and magnitude (**E**) as noted in the figure between 1.4 and 1.5 μm.

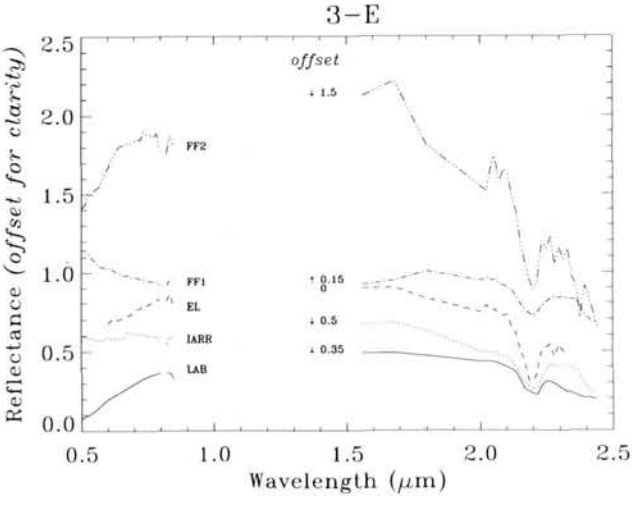

Figure 9. GER spectra for ground location 3E obtained by applying the four calibration methods (IARR, EL, FF1, and FF2). Each of the spectra was derived from exactly 86 pixels. Also shown is a laboratory spectrum of this location (LAB) resamp led into the 63 GER channels. Spectral offsets have been applied to the original spectra position (0) for clarity using different reflectance values and magnitude (**E**) as noted in the figure between 1.4 and 1.5 μm.

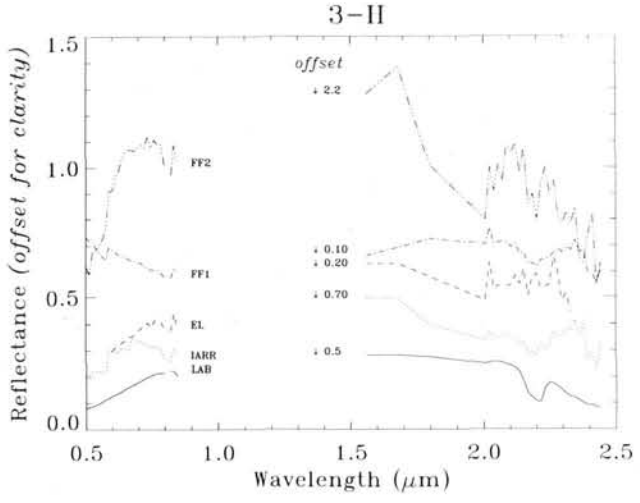

Figure 11. GER spectra for ground location 3H obtained by applying the four calibration methods (IARR, EL, FF1, and FF2). Each of the spectra was derived from exactly 28 pixels. Also shown is a laboratory spectrum of this location (LAB) resampled into the 63 GER channels. Spectral offsets have been applied to the original spectra position (0) for clarity using different reflectance values and magnitude (**E**) as noted in the figure between 1.4 and 1.5 μm.

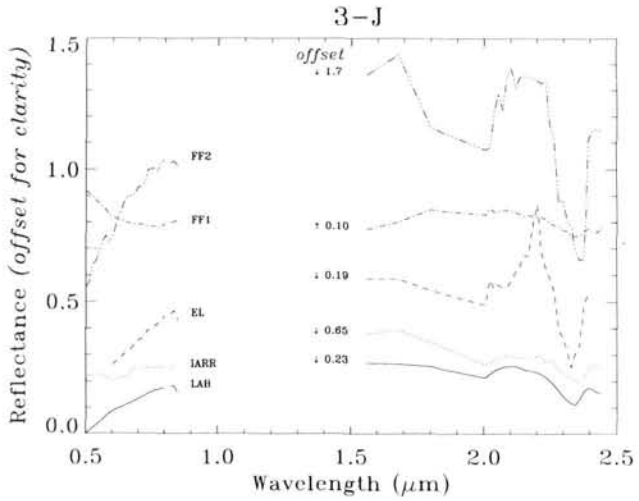

Figure 12. GER spectra for ground location 3J obtained by applying the four calibration methods (IARR, EL, FF1, and FF2. Each of the spectra was derived from exactly 100 pixels. Also shown is a laboratory spectrum of this location (LAB) resampled into the 63 GER channels. Spectral offsets have been applied to the original spectra position (0) for clarity using different reflectance values and magnitude (**E**) as noted in the figure between 1.4 and 1.5 μm.

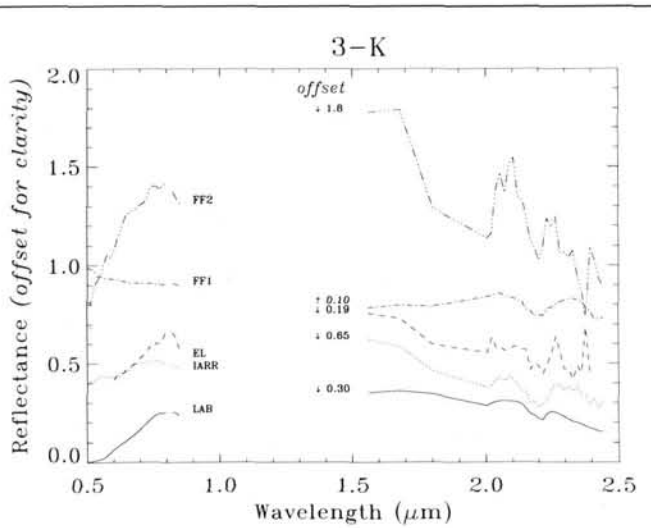

Figure 13. GER spectra for ground location 3K obtained by applying the four calibration methods (IARR, EL, FF1, and FF2). Each of the spectra was derived from exactly 74 pixels. Also shown is a laboratory spectrum of this location (LAB) resampled into the 63 GER channels. Spectral offsets have been applied to the original spectra position (0) for clarity using different reflectance values and magnitude (**E**) as noted in the figure between 1.4 and 1.5 μm.

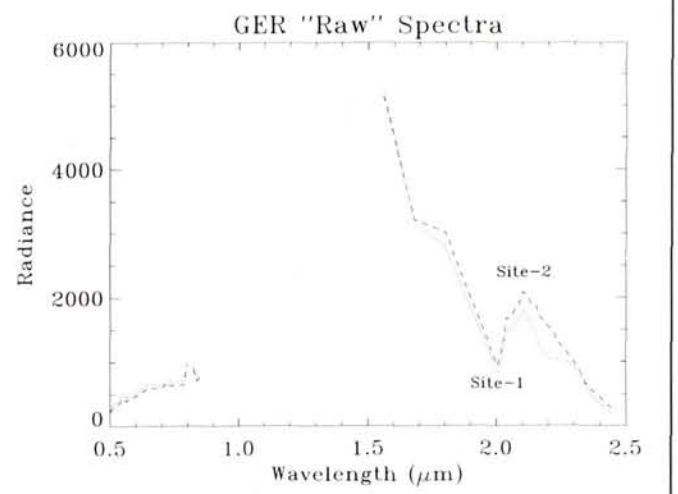

Figure 14. GER raw spectra of two different ground sites (Site-1 and Site-2) as obtained from 125 pixels before any calibration routines were applied.

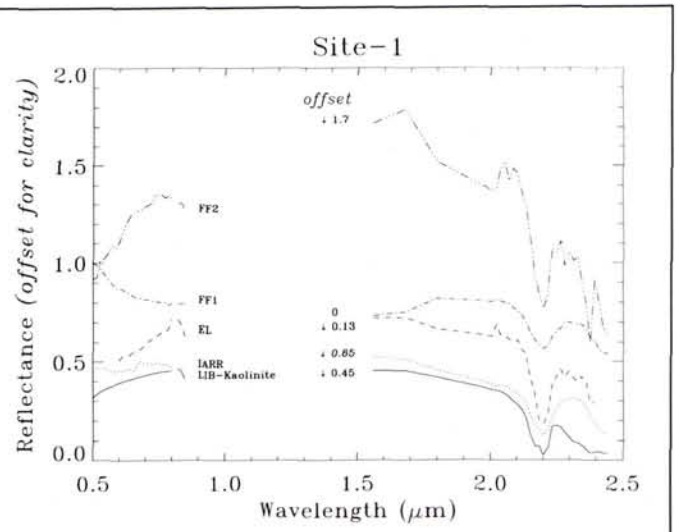

Figure 15. GER spectra obtained by applying the four calibration methods (IARR, EL, FF1, and FF2 for ground location Site-1 (using the same 125 pixels of Site-1 in Figure 14). Also shown is a SIRIS library spectrum of kaolinite (LIB) resampled into the 63 GER channels.

Mineral Mapping Using the IARR Calibration

After selection of the IARR calibration as the best means to calibrate the GER data of Makhtesh Ramon, we applied two procedures to the calibrated data to map the distribution of surface kaolinite and calcite: calibrated color composites and spectral matching. Color composite images were formed of selected bands, with the band selections being determined by the known spectral features of the endmembers. Plate 1A shows a color composite image of the IARR calibrated data with bands 5, 48, and 42 (0.526, 2.200, and 2.103 μm, re-

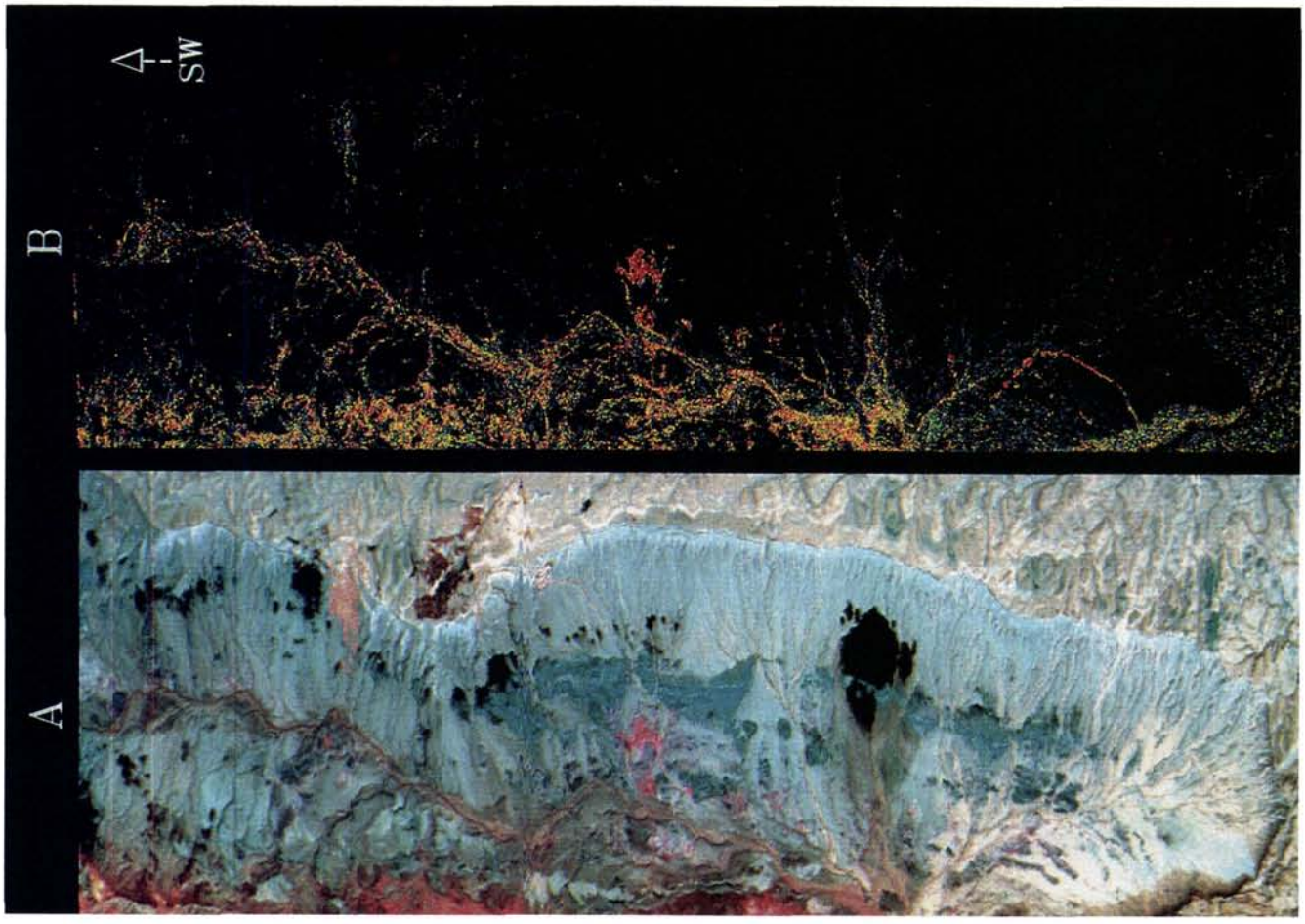

Plate 1. Images showing kaolinite distribution for Ramon-3. (A) Color composite image of the IARR calibrated data using channels 5, 48, and 42 (0.526, 2.200, and 2.103 μm, respectively). Light red to pink colors on the image represent kaolinite-rich areas. (B) Color density-sliced image of SAM results using a kaolinite endmember derived from Site-1. Red pixels represent kaolinite-rich areas.

spectively) as RGB. This color composite uses the additive red, green, and blue (RGB) color scheme to combine the three spectral bands for enhancement of the kaolinite and Fe oxides spectral features, which appear pink on the image. Plate 2A shows a similar color composite image enhancing the distribution of carbonates with bands 57, 43, and 49 (2.346, 2.119, and 2.216 μm) as RGB presenting the carbonate-rich areas as blue-green.

Spectral matching was done using the Spectral Angle Mapper (SAM) routine (CSES, 1992; Yuhas *et al.*, 1992). SAM was designed to determine the spectral similarity of the spectra in an imaging spectrometer scene to selected endmember spectra (Dr. J. W. Boardman, personal communication, 1991). This technique calculates the angular difference between two spectra treated as vectors in nb space (nb = number of bands) and produces a single image for each reference spectrum. Low values (low angular distances) in this image (displayed as bright pixels) correspond to more similar spectra, and high values (displayed as dark pixels) to less similar spectra (CSES, 1992). The two endmember spectra, each the average of 125 pixels of kaolinite (Site-1) and calcite (Site-2) were used to run the SAM procedure. The results, displayed as color density-sliced images, are presented in Plates 1B and 2B. Red areas represent the spatial distribution of those areas most spectrally similar to the selected endmembers. These image maps show the distribution of the spectrally dominant minerals and may be used to help evaluate the geologic characteristics and soils of the area. The resulting mineral maps show some correspondence to geologic units mapped by Zak (1968); however, the GER data are better suited to producing detailed soil maps because light interacts with only the upper approximately 50 μm of the ground surface area. In fact, the information being derived from the GER data of Makhtesh Ramon provides information not presently available to soil scientists for this unmapped (soil) region (Mazor, personal communication, 1992).

Conclusions

Although ground sampling occurred three years after the GER data were flown and although no field measurements were available, we were able to obtain good calibration and mapping results for the Ramon 3 GER flightline. Combined use of

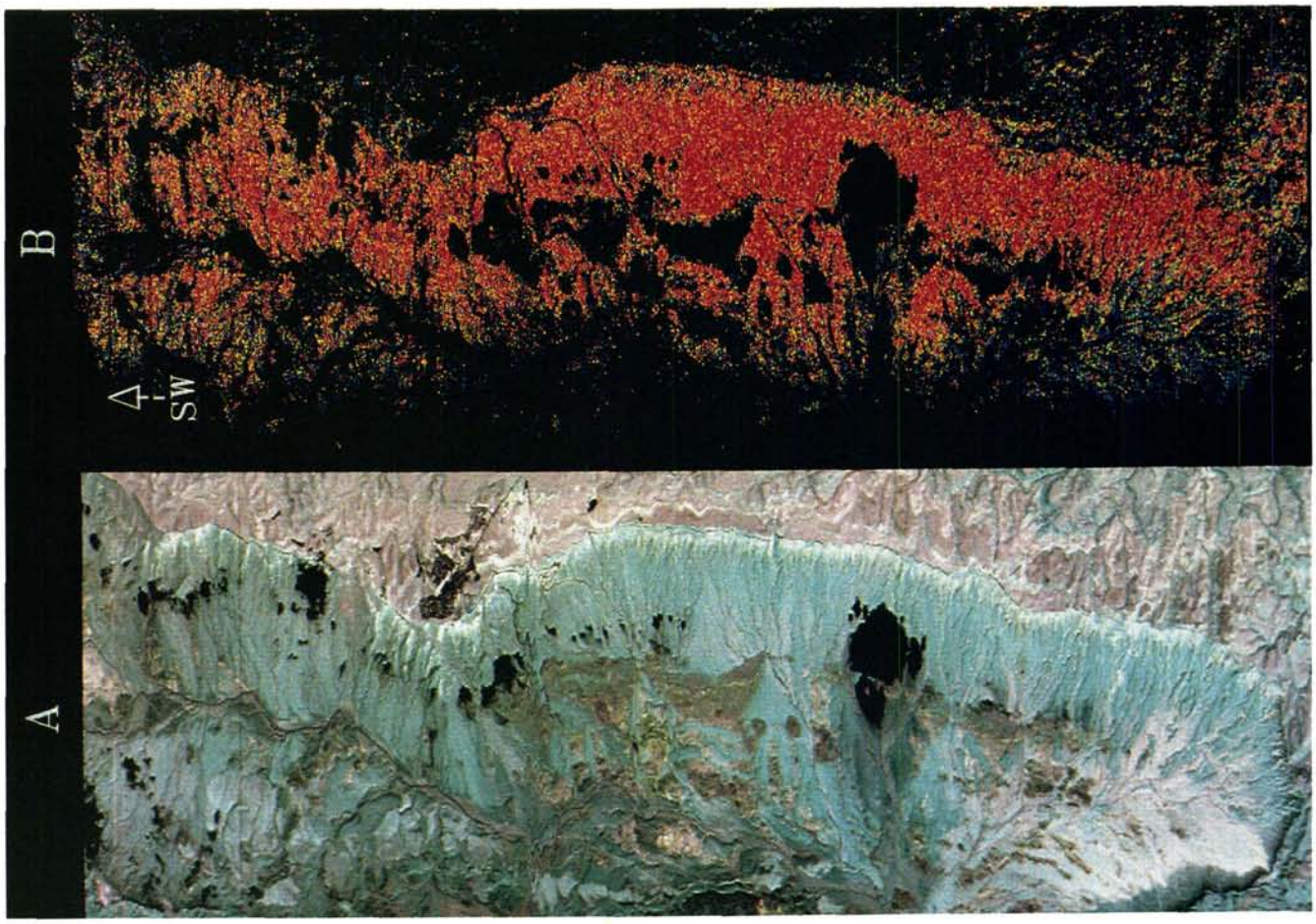

Plate 2. Images showing carbonate distribution for Ramon-3. (A) Color composite image of the IARR calibrated data using channels 57, 43, and 49 (2.346, 2.119, and 2.216, μm, respectively). Blue-green colors represent carbonate-rich areas. (B) Color density-sliced image of SAM results using a carbonate endmember derived from Site-2. Red pixels represent carbonate-rich areas.

the IARR, FF2, and EL calibrations would probably yield the best results for the Ramon-3 data. For the VNIR, the EL and the FF2 provide the best results. For the SWIR1 region, the EL calibration is the best calibration; however, poor SNR performance mandates caution when using the EL method. The IARR calibration provides the best SWIR2 results. Because combining more than one calibration method for analysis is quite complicated, we suggest using the IARR calibration as the preferred method to calibrate the entire spectral region in a given GER scene in the absence of on-site spectral measurements during the flight. The results presented here demonstrate that such an approach produces acceptable mineral spectra and reasonable mineral maps for an arid (non-vegetated) region and may help further mapping of the Makhtesh Ramon area. In all calibrations, at least for this GER data acquisition, using more than 64 pixels for calibration targets and selection of endmember spectra is highly recommended. It should be noted that better pre-flight preparation (e.g., planning for and obtaining ground reflectance and atmospheric measurements at the same time the GER data were acquired) would obviously yield even better analysis results.

Acknowledgments

The authors wish to thank the Lady Davies and Hirsch Funds for their financial support, which allowed Dr. Ben-Dor to conduct this study at CSES. We also thank Mr. R. Ben-Dor (Har-Hanegev Nature-Field School, Israel) for his assistance in ground sampling, Dr. H. Kaufmann (University of Karlsruhe, FRG) and Professor E. Mazor (The Weizmann Institute of Science, Israel) for arranging the GER flight and for their useful information, Dr. M. Shoshani (Bar-Ilan University, Israel) for providing the raw GER data, and Professor Joseph R. Smyth and Mr. Jeff R. Swope (University of Colorado) for carrying out the XRD measurements.

References

Ben-David, R., and E. Mazor, 1988. Stages in the evolution of Makhtesh Ramon and its drainage system, *Israel Journal of Earth Science*, 37:125–135.

Center for the Study of Earth from Space (CSES), 1992. *SIPS User's Guide, Spectral Image Processing System Version 1.1*, University of Colorado, Boulder, 74 p.

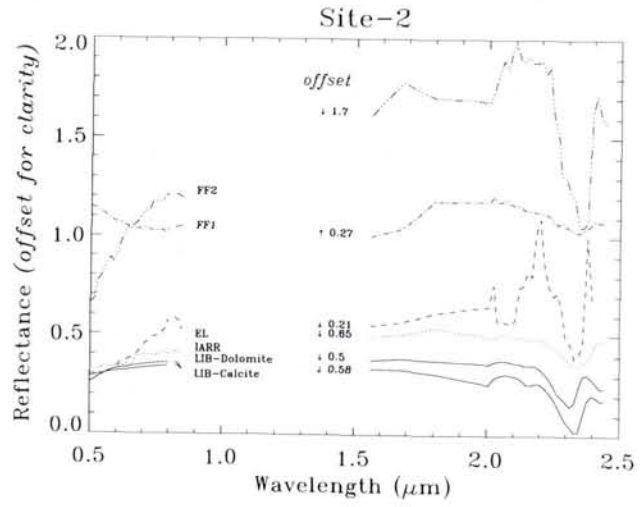

Figure 16. GER spectra obtained by applying the four calibration methods (IARR, EL, FF1, and FF2) for ground location Site-2 (using the same 125 pixels of Site-2 in Figure 14). Also shown is a SIRIS library spectrum of dolomite (LIB) resampled into the 63 GER channels.

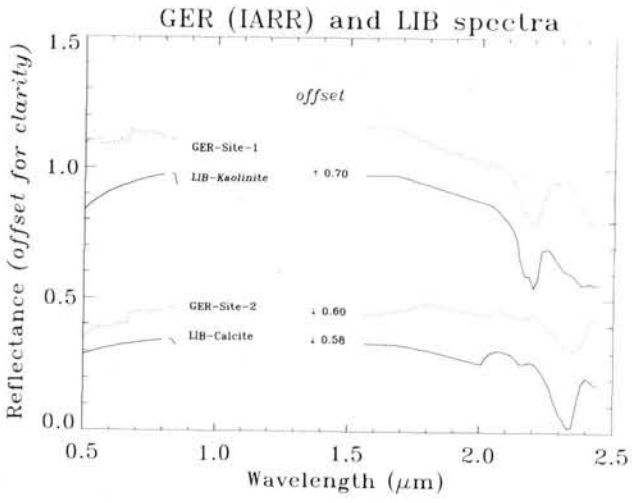

Figure 17. GER spectra of ground locations Site-1 and Site-2 obtained by applying the IARR calibration (using the same 125 pixels of both Sites in Figure 14) compared to SIRIS library spectra (LIB) of kaolinite and calcite, respectively.

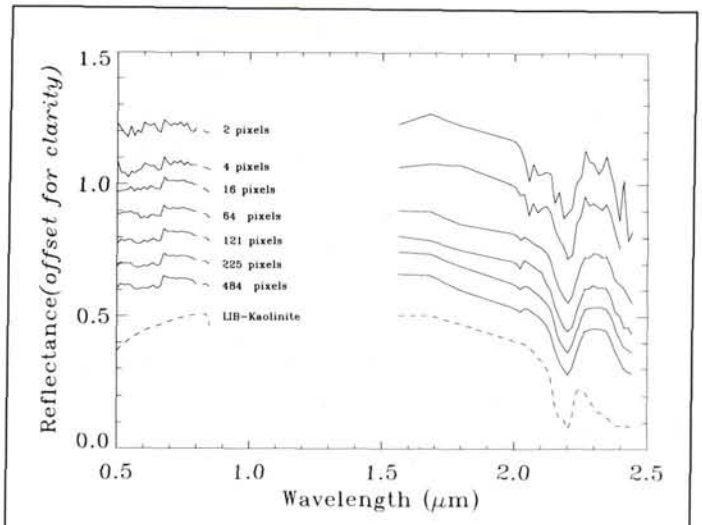

Figure 18. GER spectra of ground location Site-1 derived from averaging different numbers of homogeneous pixels. Also shown is a SIRIS library spectrum of kaolinite (LIB) resampled into the 63 GER channels.

Collins, W.E., and S.H. Chang, 1985. First results from a new multichannel, narrow band IR scanner, *Proceedings of the 4th Thematic Conference, Remote Sensing for Exploration Geology.*

———, 1988. Application of Geophysical Environmental Research (GER) airborne scanner data for detection of hydrothermal alteration in Nevada, *Proceedings of the 6th Thematic Conference on Remote Sensing for Exploration Geology,* Summaries, pp. 14–15.

———, 1990. The Geophysical Environmental Research Corp. 63 channel airborne imaging spectrometer and 12 band thermal scanner, *Proceedings of The International Society for Optical Engineering, Imaging Spectroscopy of the Terrestrial Environment,* 1298:62–71.

Conel, J.E., 1985. Calibration of data using ground-based spectral reflectance measurements, *Proceedings of Airborne Imaging Spectrometer Data Analysis Workshop,* 15 September, JPL Publication 85-41, Jet Propulsion Laboratory, Pasadena, California, pp. 184–85.

Conel, J.E., R.E. Green, C.J. Alley, V. Bruegge, J.S. Carrere, G. Margolis, G. Vane, T.G. Chrien, P.N. Slater, S.F. Biggar, P.M. Teillet, R.D. Jackson, and M.S. Moran, 1988. In-flight radiometric calibration of the Airborne Visible/Infrared Imaging Spectrometer (AVIRIS), *Proceedings SPIE Conference on Recent Advances on Sensors, Radiometry and Data Processing for Remote Sensing,* 924:168–178.

Crowley, J., 1990. Techniques for AVIRIS data normalization in areas with partial vegetation cover, *Proceedings of the Second Airborne Visible/Infrared Imaging Spectrometer (AVIRIS) Workshop.* JPL Publication 90-54 , Jet Propulsion Laboratory, Pasadena, California, pp. 192–198.

Crowley J., K. Rowan, and M. Podwysocki, 1988. Evaluation of Airborne Visible/ Infrared Imaging Spectrometer (AVIRIS) data of the Mountain Pass, California carbonatite complex, *Proceedings of the Airborne Visible/Infrared Imaging Spectrometer (AVIRIS) Performance Evaluation Workshop,* JPL Publication 88-38, Jet Propulsion Laboratory, Pasadena, California, pp. 155–161.

Elvidge, C. D., 1988. Vegetation reflectance features in AVIRIS data, *Proceedings, International Symposium on Remote Sensing of Environment, Sixth Thematic Conference, "Remote Sensing for Exploration Geology,"* Houston Texas, 16–19 May, Environmental Research Institute of Michigan, Ann Arbor, pp. 169–182.

Gaffey, S. J., 1986. Spectral reflectance of carbonates in the visible and near infrared (0.35-2.55μm); calcite, aragonite and dolomite: *American Mineralogist,* 71:151–162.

Gao, B., and A. F. H. Goetz, 1990. Column atmospheric water vapor and vegetation liquid water retrievals from airborne imaging spectrometer data, *Journal of Geophysical Research,* 95:D4,3549–3564.

Geophysical and Environmental Research (GER), 1988. *The Single Beam Visible/InfraRed Intelligent Spectroradiometer (SIRIS) User's Manual.*

Goetz, A.F.H., and V. Srivastava, 1985. Mineralogical mapping in the Cuprite mining district, Nevada, *Proceedings of Airborne Imaging Spectrometer (AIS) Data Analysis Workshop*, 8–10 April, JPL Publication 85-41, Jet Propulsion Laboratory, Pasadena, California, pp. 22–31.

Green, A.A, and M.D. Craig, 1985. Analysis of aircraft spectrometer data with logarithmic residuals, *Proceedings of the Airborne Imaging Spectrometer Data Analysis Workshop*, JPL Publication 85-41, Jet Propulsion Laboratory, Pasadena, California, pp. 111–119.

Green, R.O, Gregg Vane, and J.E. Conel, 1988. Determination of in-flight AVIRIS spectral, radiometric, spatial and signal-to-noise characteristics using atmospheric and surface measurements from the vicinity of the rare-earth-bearing carbonatite at Mountain Pass, California, *Proceedings of the Airborne Visible/Infrared Imaging Spectrometer (AVIRIS) Performance Evaluation Workshop*, JPL Publication 88-38, Jet Propulsion Laboratory, Pasadena, California, pp. 62–184.

Grove, C. I., S.J. Hook, and E.D. Paylor, 1992. *Laboratory reflectance spectra of 160 minerals, 0.4 to 2.5 micrometers*, JPL Publication 92-2, Jet Propulsion Laboratory, Pasadena, California, 300 p.

Hunt, G. R., and J. W. Salisbury, 1970. Visible and near infrared spectra of rocks. I. Silicate minerals, *Modern Geology*, 1:283–300.

Hauff, P. L., and F.K. Kruse, 1990. Spectral identification and characterization (1.2 - 2.5 μm) of kaolinite/smectite clays in weathering environments, *Proceedings, Australasian Remote Sensing Conference, 5th*, Perth, Western Australia, pp. 898–905.

Kaufmann, H., W. Weisbrich, M. Beyth, Y. Bartov, A. Itamar, E. Mazor, S. Ronen, and U. Kafri, 1991. Mineral identification using GER-II data acquired from Makhtesh Ramon/Negev, Israel. *EARSel Advances in Remote Science*, 1:82–92.

Kneizys, F.X., G.P. Anderson, E.P. Shettle, W.O. Gallery, L.W. Abreu, J.E.A. Selby, J.H. Chetwynd, and S.A. Clough, 1988. *User Guide to LOWTRAN-7*, Environmental Research Papers No. 1010, AFGL-TR-88-0177, Air-Force Geophysical Laboratories.

Kruse, F. A., 1988. Use of airborne imaging spectrometer data to map minerals associated with hydrothermally altered rocks in the northern Grapevine Mountains, Nevada and California, *Remote Sensing of Environment*, 24(1):pp. 31–51.

Kruse, F. A., W.M. Calvin, and O. Seznec, 1988. Automated extraction of absorption features from Airborne Visible/Infrared Imaging Spectrometer (AVIRIS) and Geophysical Environmental Research imaging spectrometer (GERIS) data, *Proceedings of the Airborne Visible/Infrared Imaging Spectrometer (AVIRIS) performance evaluation workshop*, JPL Publication 88-38, Jet Propulsion Laboratory, Pasadena, California, pp. 62–75.

Kruse, F. A., and P.L. Hauff (editors), 1993. *The IGCP-264 Spectral Properties Database: IUGS/UNESCO*, Special Publication, 211 p. (in press).

Kruse, F. A., K.S. Kierein-Young, and J.W. Boardman, 1990. Mineral mapping at Cuprite, Nevada with a 63 channel imaging spectrometer, *Photogrammetric Engineering & Remote Sensing*, 56(1): 83–92.

Kruse, F. A., A.B. Lefkoff, J.B. Boardman, K.B. Heidebrecht, A.T. Shapiro, P.J. Barloon, and A.F.H. Goetz, 1993. The Spectral Image Processing System (SIPS) - Interactive Visualization and Analysis of Imaging Spectrometer Data, *Remote Sensing of Environment*, Special issue on AVIRIS, 44:145–163.

Kruse, F. A., G.L. Raines, and K. Watson, 1985. Analytical techniques for extracting geologic information from multichannel airborne spectroradiometer and airborne imaging spectrometer data, *Proceedings, International Symposium on Remote Sensing of Environment Fourth Thematic Conference, "Remote Sensing for Exploration Geology,"* San Francisco, California, 1–4 April, pp. 309–324.

Lehmann, F., S. Mackin , R. Richter, H. Rothfuss, and A. Waldbrotd, 1990. The European imaging spectrometry campaign 1989 (EISAC) - preprocessing and evaluation of the GER airborne imaging spectrometer data, *Progress Report to the European Community*, JRC, Ispra, DLR-552-14/89, DLR Institute for Optoelectronics, Oberpfaffenhofen, FRG.

Lillesand, T.M., and R. W. Kiefer, 1979. *Remote Sensing and Image Interpretation*, John Wiley & Sons, N.Y., pp. 423-425.

Mackin, S., and T.J. Munday, 1988. *Imaging Spectrometry in Environmental Science Research and Applications—Preliminary Results from the Analysis of GER-II Imaging Spectrometer Data—Australia and the USA*, Dept. of Geological Sciences, University of Durham, Durham, England, Interim Report 1, Contract No.: D/ER1/9/4/2052/40/RAE(F) BNSC, 44 p.

Mazor, E., and S. Shoval, 1987. Makhtesh Ramon as a geological museum, *Geological Field Trips in the Makhtesh Ramon Area, Israel Geologic Society Annual Meeting* (Y. Brtov, editor), Mizpe Ramon, pp. 1–5.

McKie, D., and C. McKie, 1986. X-Ray powder diffraction patterns, *Essentials of Crystallography*, Blackwell Scientific Publication, Oxford-London-Edinburgh-Boston-Palo Alto-Melbourne, pp. 227-231.

Podwysocki, M., and O. Jones, 1988. Airborne imaging spectrometer and mineral mapping, *The CROSS SECTION*, USGS, Geologic Division, pp. 37–40.

Rast, M., S.J. Hook, C.D. Elvidge, and R.C. Alley, 1991. An evaluation of techniques for the extraction of mineral absorption features from high spectral resolution remote sensing data, *Photogrammetric Engineering & Remote Sensing*, 57(10):1303–1309.

Roberts, D. A., Y. Yamaguchi, and R.J.P. Lyon, 1985. Calibration of airborne imaging spectrometer data to percent reflectance using field spectral measurements, *Proceedings of the Nineteenth International Symposium on Remote Sensing of Environment*, Ann Arbor, Michigan, 21–25 October.

Vane, Gregg, T.G. Chrien, E.A. Miller, and J.H. Reimer, 1987. Spectral and radiometric calibration of the Airborne Visible/Infrared Imaging Spectrometer (AVIRIS), *Proceedings of SPIE-The International Society for Optical Engineering, Imaging Spectroscopy II*, 834:91–105.

Weidner, V. R., and J. J. Hsia, 1981. Reflection properties of pressed polytetrafluoroethylene powder, *Journal of Optics Society of America*, 71:856–859.

Werner, K., and F. Lehmann, 1991. EISAC'89: Evaluation of GER airborne scanner data in the Almaden testsite (Spain), *EARSel Advances in Remote Sensing*, 1:43–57.

Yuhas, R. H, A. F. H. Goetz, and J. W. Boardman, 1992. Discrimination among semi-arid landscape endmembers using the Spectral Angle Mapper (SAM) algorithm, *Summaries of the Third Annual JPL Airborne Geoscience Workshop*, JPL Publication 92-14, 1:147-149.

Zak, I., 1968. *Geologic Map of Israel, Makhtesh Ramon, Har Gevanim, 1:20,000 scale*, Geological Survey of Israel.

———, 1987. The structure of Ramon arch and the Ramon line, southern Israel, *Israel Geologic Society Annual Meeting*, Mizpe Ramon, pp. 145–147.

Zamudio, J.A., and W.W. Atkinson, 1990. Analysis of AVIRIS data for spectral discrimination of geologic materials in the Dolly Varden Mountains, Nevada, *Proceedings of the Second Airborne Visible/Infrared Imaging Spectrometer (AVIRIS) Workshop*, JPL Publication 90-54, Jet Propulsion Laboratory, Pasadena, California, pp. 162–166.

(Received 10 November 1992; accepted 3 March 1993, revised 8 April 1993)

Eyal Ben-Dor

Eyal Ben-Dor received the B.S. degree (Cum Laude) in Agriculture Science in 1983 from the Hebrew University of Jerusalem, Israel. He earned both the M.S. (Cum Laude) (1986) and Ph.D. (1992) in Soil Sciences, also from the Hebrew University of Jerusalem, Israel. He is currently conduct-

ing postdoctoral research at the Center for the Study the Earth from Space (CSES), University of Colorado at Boulder. He has been selected as a Visiting Fellow of the Cooperative Institute for Research in Environmental Sciences (CIRES) for 1993-94. Dr. Ben-Dor's expertise is in the areas of soil chemistry, mineralogy, and surface properties of soil materials. His research includes developing techniques to quantitatively predict soil constituents from their diffuse reflectance in the visible, near infrared, and short wave infrared spectral regions. His current research is adapting these quantitative models for use with high resolution imaging data to remotely derive soil chemistry.

Fred A. Kruse

Dr. Fred Kruse received the B. S. degree in geology from the University of Massachusetts, Amherst, in 1976. He earned both the M.S. (1984) and Ph. D. degrees (1987) in geology from the Colorado School of Mines, Golden, Colorado. Dr. Kruse served as a Topographic Engineer Officer in the United States Army Corps of Engineers (1976 to 1981) and with the Remote Sensing Section of the U. S. Geological Survey, Branch of Geophysics (1982–1987). He is presently Deputy Director, Center for the Study of Earth from Space (CSES); Fellow, Cooperative Institute for Research in Environmental Sciences (CIRES); and Assistant Research Professor, Department of Geological Sciences, all within the University of Colorado, Boulder. Dr. Kruses's primary research interests are in the application of remote sensing technology to the areas of ore deposits, their regional occurrence and distribution, and geologic evolution. Supporting research includes development of visualization techniques for interactive image analysis, use of artificial intelligence (AI) techniques for identifying and mapping Earth-surface materials, and extraction and practical use of quantitative information from combined optical and Radar remote sensing data to address geologic problems relating to geomorphic development of the land surface. Dr. Kruse is a member of the Shuttle Imaging Radar-C (SIR-C) Science Team.

Adam B. Lefkoff

Mr. Adam B. Lefkoff is a 1990 graduate of the University of California, San Diego, with a B.A. in Computer Science (Cum Laude). While at UCSD, he was the recipient of an Education Abroad Scholarship, which allowed him to spend a year at Flinders University of South Australia (1989–90). Presently, Mr. Lefkoff is an independent consultant and author of a commercial software system for interactive analysis and visualization of multispectral remote sensing data and other raster images. At the time this paper was written, Mr. Lefkoff was a Senior Applications Programmer (1990–93) at the Center for the Study of Earth from Space (CSES), Cooperative Institute for Research in Environmental Sciences (CIRES), University of Colorado, Boulder, Colorado. He was the lead programmer for development of the Spectral Image Processing System (SIPS) and the Radar Analysis and Visualization Environment (RAVEN), two showcase interactive image processing systems written in the Interactive Data Language (IDL).

Amos Banin

Amos Banin, Columbia Foundation Professor of Soil and Water Sciences

Born: Jerusalem, 1935. Ph.D.: Hebrew University of Jerusalem, 1965.

Hebrew University: Lecturer, 1967; Senior Lecturer, 1970; Associate Professor, 1974; Professor, 1978. Other Appointments: Visiting Asst. Prof., Purdue Univ., 1964–66; Visiting Scientist, U.S. Army Cold Regions Research and Eng. Lab., Hanover, N.H., 1972–73; Senior Research Assoc., Univ. of Washington, Seattle, Washington, 1973–74; NASA-Ames Research Center, Calif., 1982–84; Adjunct Prof., San Francisco St. Univ., since 1984; Member, Soil Science Soc. of Amer., Clay Minerals Soc., Int'l. Soil Science Soc.; Co-Chairperson, Commission F-4, the International Committee on Space Research (COSPAR), since 1986.

Research interests: Science and technology of soils and clays; the role of soils in global planetary processes on earth and other planets.